Demethylmenaquinol is a substrate of *Escherichia coli* nitrate reductase A (NarGHI) and forms a stable semiquinone intermediate at the NarGHI quinol oxidation site

CrossMark

Julia Rendon [a,1], Eric Pilet [a,c,1], Zeinab Fahs [a,b,2], Farida Seduk [b], Léa Sylvi [b,3], Mahmoud Hajj Chehade [d,e], Fabien Pierrel [d,e], Bruno Guigliarelli [a], Axel Magalon [b,*], Stephane Grimaldi [a,**]

[a] Aix-Marseille Université, CNRS, Unité de Bioénergétique et Ingénierie des Protéines (UMR7281), F-13402 Marseille, France
[b] Aix-Marseille Université, CNRS, Laboratoire de Chimie Bactérienne (UMR7283), F-13402 Marseille, France
[c] Université Pierre et Marie Curie, Faculté de Biologie (UFR927), F-75005 Paris, France
[d] Université Grenoble Alpes, Laboratoire Adaptation et Pathogénie des Microorganismes (LAPM), F-38000 Grenoble, France
[e] Centre National de la Recherche Scientifique (CNRS), LAPM, F-38000 Grenoble, France

ARTICLE INFO

ABSTRACT

Quinones are essential building blocks of respiration, a universal process dedicated to efficient harvesting of environmental energy and its conversion into a transmembrane chemiosmotic potential. Quinones differentiate mostly by their midpoint redox potential. As such, γ-proteobacteria such as *Escherichia coli* are characterized by the presence of demethylmenaquinone (DMK) with an intermediate redox potential between low-potential (menaquinone) and high-potential (ubiquinone) quinones. In this study, we show that demethylmenaquinol ($DMKH_2$) is a good substrate for nitrate reductase A (NarGHI) in nitrate respiration in *E. coli*. Kinetic studies performed with quinol analogs on NarGHI show that removal of the methyl group on the naphthoquinol ring impacts modestly the catalytic constant but not the K_M. EPR-monitored redox titrations of NarGHI-enriched membrane vesicles reveal that endogeneous demethylmenasemiquinone (DMSK) intermediates are stabilized in the enzyme. The measured midpoint potential of the DMK/$DMKH_2$ redox couple in NarGHI ($E'_{m,7.5}$ (DMK/$DMKH_2$) ~ -70 mV) is significantly lower than that previously measured for unbound species. High resolution pulsed EPR experiments demonstrate that DMSK are formed within the NarGHI quinol oxidation site. Overall, our results provide the first characterization of a protein-bound DMSK and allows for comparison for distinct use of three quinones at a single Q-site in NarGHI.

© 2015 Elsevier B.V. All rights reserved.

1. Introduction

Living organisms have developed multiple strategies to harvest environmental energy and convert it into a transmembrane chemiosmotic potential used for ATP synthesis. In the overwhelming majority of cases, this is achieved by electron transport chains which are fuelled by electrochemical disequilibria between reducing and oxidizing substrates present in the extracellular environment or generated by cell metabolism [1]. Prokaryotes can use a diverse range of organic and inorganic substrates to donate or accept electrons at various electrochemical potentials [2]. For instance, the gut bacterium *Escherichia coli* possess a number of respiratory complexes supporting growth on a variety of alternative terminal electron acceptors to oxygen such as nitrate, nitrite, fumarate, dimethyl sulfoxide or trimethylamine *N*-oxide [3,4]. With the exception of specific types of acetogenesis and methanogenesis, all bioenergetic chains rely on the use of small, lipophilic quinone molecules diffusing across the membrane and constituting the so-called quinone pool connecting respiratory complexes. In most cases, quinones receive or donate electrons from or to one-electron carriers such as

hemes or FeS centers. However, depending on their environment within Q-sites of respiratory complexes, they can act as one-electron or two-electron redox couples with the congruent stabilization of semiquinone intermediates [5]. Importantly, prokaryotes make use of low-potential and/or high-potential quinones to define preferred electron routes towards terminal electron acceptors. In this context, *E. coli* synthesizes three different respiratory quinones which differ not only by their chemical structure (Fig. 1A–B), but also with respect to their two-electron midpoint redox potential value $E'_{m,7}$ (Q/QH$_2$): a low-potential quinone (menaquinone or MK with an $E'_{m,7} = -70 \pm 10$ mV), a high-potential one (ubiquinone or UQ with an $E'_{m,7} = +100 \pm 10$ mV) and an intermediate one (demethylmenaquinone or DMK with an $E'_{m,7} = +36$ or -7 mV depending on the literature [6,7]). DMK differs from MK by the lack of the methyl group at the C2 position of the quinone ring (Fig. 1A). Considering the required redox potential difference between the reductant and the oxidant for chemiosmosis, high-potential UQ is the preferred electron carrier in aerobic respiration, whereas low-potential quinones (MK and DMK) are mainly involved in anaerobic respiration. However, DMK has been recently recognized to be involved in aerobic respiration as well in *E. coli* [8]. The proportion of UQ, MK and DMK in the *E. coli* quinone pool varies depending on the nature of the electron acceptor, the growth phase, and the available carbon source [9–13], contributing to maintain metabolic flexibility in response to environmental changes.

The ability of some facultative anaerobes from the γ-proteobacteria class such as *E. coli* to synthesize both low-potential and high-potential quinones opened up the possibility to investigate *in vivo* the specificity of quinone utilization by respiratory complexes. The respiratory nitrate reductase complex (NarGHI) from *E. coli* is an excellent model for studying these questions since it was shown to oxidize both MKH$_2$ and UQH$_2$, but, surprisingly, not DMKH$_2$ [13,14]. This heterotrimeric cytoplasmically-oriented complex is composed of (i) a nitrate-reducing subunit NarG containing a Mo-*bis*-PGD cofactor and a [4Fe–4S] cluster, (ii) an electron-transfer subunit NarH carrying four FeS clusters, and (iii) a membrane anchor subunit NarI containing two *b*-type hemes termed b_D and b_P according to their distal and proximal positions with respect to the nitrate reducing site [15]. We have demonstrated that NarGHI stabilizes menasemiquinone (MSK) and ubisemiquinone (USQ) intermediates at a single quinol oxidation site Q$_D$ located within the NarI subunit close to heme b_D [16–19]. Moreover, the use of high resolution pulsed EPR methods in combination with isotopic enrichment strategies allowed us to resolve a strongly asymmetric binding mode of MSK at the Q$_D$ site (referred to as MSQ$_D$) via the

formation of a single short hydrogen bond to the heme b_D axial ligand His66 [20,21] and the same binding mode likely occurs for USQ [16] (Fig. 1D).

In this work, we describe the participation of DMK in NarGHI-supported respiration using an *E. coli* strain that contains DMK as its sole respiratory quinone. Our results demonstrate that DMK is a substrate to NarGHI and that the absence of a methyl group at the C2 position of the quinone ring has a moderate effect on its utilization by the enzyme. Furthermore, the use of DMK is coupled with stabilization within the NarGHI Q$_D$ site of a demethylmenasemiquinone (DMSK) intermediate displaying peculiar redox and spectroscopic properties. The ability of this respiratory complex to utilize all three natural quinones in *E. coli* offers the unique possibility to investigate structure–function relationships of quinone reactivity.

2. Material and methods

2.1. Bacterial strains, plasmids and growth conditions

The *E. coli* strains and plasmids used in this study are described in Table 1. *E. coli* strains were routinely grown aerobically in Luria Broth medium at 37 °C supplemented with antibiotics when necessary. The *ubiE* gene was inactivated in MG1655 and in the nitrate reductase-deficient JCB4023 strain using P1 transduction from the JW5581 strain of the Keio collection [23]. The kanamycin-resistance cassette was further eliminated from the MG1655*ubiE* transductant strain with the use of pCP20 plasmid encoding the FLP recombinase. Using the same procedure, the *ubiA* (resp. *menA*) gene involved in the initial steps of UQ (resp. DMK) biosynthesis was inactivated in the MG1655 strain. The MG1655*ubiA* strain was used subsequently for inactivation of the *ubiE* gene. Growth was also performed at 37 °C in defined minimal medium supplemented with 137 mM glycerol (unless stated elsewhere in the text) used as sole carbon source either aerobically or in anaerobic conditions using gas tight hungate tubes under Ar atmosphere. For anaerobic growth under nitrate-respiring conditions, nitrate was added at 100 mM final concentration and used as terminal electron acceptor. The minimal medium is composed of potassium phosphate buffer (100 mM) adjusted at pH 7.4, ammonium sulfate (15 mM), NaCl (9 mM), magnesium sulfate (2 mM), sodium molybdate (5 μM), Mohr's salt (10 μM), and calcium chloride (100 μM). After filtration, casaminoacids (0.5%) and thiamine (0.01%) were added just before use together with antibiotics, if necessary.
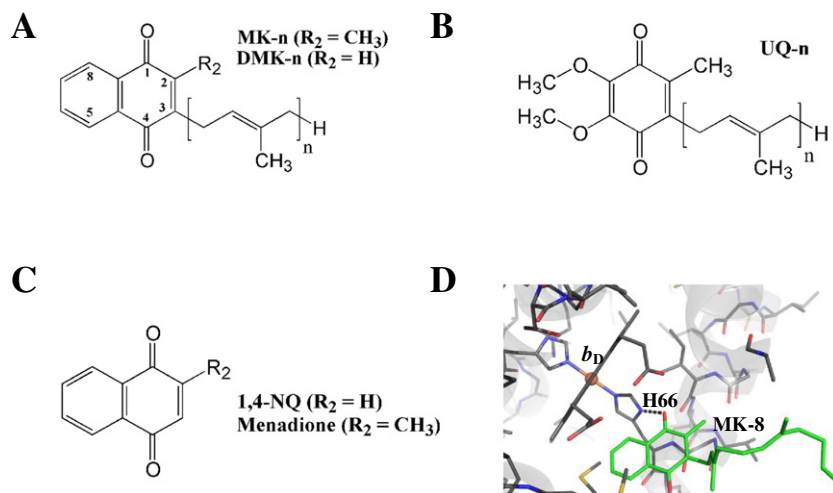
Fig. 1. Molecular structure of respiratory isoprenoid quinones synthesized by *E. coli* and of their analogs used in this work. A) MK-n and DMK-n, and B) UQ-n. The major species found in the bacterium has n = 8 prenyl units. C) 1,4-NQ and menadione. D) Working model of MSQ$_D$ binding mode in *E. coli* NarGHI based on our previous spectroscopic work [20,21] and using the crystal structure of NarGHI in complex with pentachlorophenol (PDB ID: 1Y4Z) as a template [22]. His66 coordinates heme b_D and hydrogen bonds with MSK.

Table 1
Bacterial strains and plasmids used in this study.

Strain or plasmid	Relevant genotype	Reference
Strains		
MG1655	Parental strain	Lab collection
MG1655*ubiE*	MG1655, Δ*ubiE*	L. Loiseau
MG1655*ubiEA*	MG1655, Δ*ubiE*::Cm^R, Δ*ubiA*::Kan^R	L. Loiseau
MG1655*menA*	MG1655, Δ*menA*	L. Loiseau
JCB4023	RK4353, Δ*napA–B*, *narG*::*ery*, Δ*narZ*::Ω, Spc^R	[24]
JCB4023*ubiE*	JCB4023, Δ*ubiE*::Kan^R	This study
JW5581	BW25113, Δ*ubiE*::Kan^R	Keio collection
Plasmids		
pCP20	encodes FLP-recombinase, Cm^R, Amp^R	[25]
pVA700	pJF119EH, P$_{tac}$-(*narGHJI*), Amp^R	[26]

Overproduction of NarGHI was achieved using the pVA700 plasmid [26]. *E. coli* strains transformed with the pVA700 plasmid were grown semi-aerobically in Terrific Broth at 37 °C as described in [18] supplemented by 0.2 mM of isopropyl 1-thio-β-D-galactopyranoside to induce the *narGHJI* expression.

2.2. Preparation of membrane fractions

Purified *E. coli* inner membrane vesicles (IMVs) were prepared as described in [18], using a buffer containing 100 mM MOPS and 5 mM EDTA at pH 7.5, frozen in liquid N$_2$ and stored at −80 °C until use. Deuterium-exchanged samples were prepared using the same membrane extraction protocol with a buffer containing ^{2}H$_2$O (99.9%, purchased from Sigma Aldrich). Protein concentration in IMVs was measured by the method of Lowry et al. [27] whereas NarGHI quantitation in NarGHI-enriched IMVs was achieved using rocket immunoelectrophoresis as described in [28,29]. NarGHI concentration was estimated between 80 and 280 μM, depending on preparations.

2.3. Enzyme assays and quinone analysis

Nitrate reductase activity was measured spectrophotometrically using quinol analogs as electron donors [30,31]. Quinol:nitrate oxidoreductase activity was followed at 360 nm in an anaerobic chamber at 25 °C. Menadiol and 1,4-naphthoquinol (1,4-NQ) were used as analogs of MKH$_2$ and DMKH$_2$, respectively (Fig. 1C), and 1.8 and 2 mM^{-1} cm^{-1} were considered for their respective molar extinction coefficient value. Steady-state kinetic studies were performed as follows. Assays were carried out in N$_2$-saturated 100 mM MOPS, 5 mM EDTA, pH 7.5, using 2 mL cuvettes. Zinc-reduced quinol was added to a buffer-filled cuvette followed by the NarGHI-enriched IMV suspension. After equilibration, the reaction was initiated by the addition of saturating amount of nitrate (15 mM) and thorough mixing in the cuvette. The stability of the reduced quinone in ethanolic solution was assessed by recording optical spectra before and after the assays in the anaerobic chamber. No change was observed under these conditions. The activity was measured using twelve different quinone concentrations up to 250 μM. Each measurement was repeated six times. Experimental kinetic data were fitted to Michaelis–Menten equations by non-linear least squares using OriginPro 8.1 (OriginLab Corporation, Northhampton, MA).

To analyze the quinone content of IMVs, quinones were extracted from IMVs (160–400 μg proteins) in glass tubes with 1.8 mL methanol and 1.2 mL petroleum ether (60 °C boiling range) as described in [32]. UQ-10 was added as an internal standard before the extraction and dried lipid extracts were analyzed by HPLC coupled to electrochemical detection (HPLC-ECD) as described in [32] except that the potentials used on the 5011A detection cell were E1, −800 mV and E2, +800 mV. The peaks corresponding to MK and DMK were integrated and the values were directly compared to estimate the MK/DMK ratio (see SI information).

2.4. Redox titrations and EPR spectroscopic studies

Redox titrations of IMVs were carried out anaerobically as previously described [18]. The following redox mediators were used at 10 μM final concentrations: 2,6-dichloroindophenol (+217 mV), 2,5-dimethy-*p*-benzoquinone (+180 mV), 1,2-naphthoquinone (+145 mV), phenazine methosulfate (+80 mV), phenazine ethosulfate (+55 mV), methylene blue (+11 mV), resorufine (−51 mV), indigocarmine (−125 mV), anthraquinone 2,6-disulfonate (−184 mV) and phenosafranine (−252 mV). All redox potentials are given in the text with respect to the standard hydrogen electrode. Cw EPR measurements were performed on a Bruker ElexSys E500 spectrometer. Low-temperature X-band EPR spectra were recorded using a standard rectangular Bruker cavity (ST 4102) fitted to an Oxford Instruments Helium flow cryostat (ESR900). The semiquinone content was quantitated relative to the Fe$_3$S$_4$ cluster (FS4) content measured in a fully ox-idized sample using double integration of their respective EPR signal recorded in non-saturating conditions. Plotted against the ambient redox potential E, this spin intensity ratio R_{SQ} was fitted to a theoretical curve corresponding to two successive one-electron redox processes:

$$R_{SQ} = \frac{R_{occ}}{1 + e^{\alpha(E-E_1)} + e^{\alpha(E_2-E)}} \tag{1}$$

where α = F/RT. E_1 and E_2 are the midpoint potentials of the n = 1 Q/SQ and SQ/QH$_2$ couples, respectively, R and F are the molar and Faraday constants, respectively, and T is absolute temperature. R_{occ} is the occupancy level of the Q$_D$ site. It corresponds to the fraction of the site occupied by either Q, SQ or QH$_2$. The midpoint potential of the n = 2 Q/QH$_2$ couple, which corresponds to the maximal amount of SQ, is $E_m = (E_1 + E_2)$ / 2. The SQ stability constant K_S defined with respect to the conproportionation reaction is:

$$K_S = \frac{[SQ]^2}{[Q][QH_2]} = e^{\alpha(E_1-E_2)}. \tag{2}$$

Differences in the binding constants of Q (K_Q) and QH$_2$ (K_{QH2}) manifest as a shift in the E_m from that of free Q/QH$_2$ given by

$$E_{m(bound)} - E_{m(free)} = \alpha/2 \cdot \ln(K_{QH2}/K_Q). \tag{3}$$

The affinity of the site for SQ is a determinant of E_1 and E_2 but not of E_m.

Analysis of microwave progressive power saturation data was carried out by computer fitting to the empirical equation

$$I = \frac{AP^{1/2}}{\left(1 + \frac{P}{P_{1/2}}\right)^{b/2}} \tag{4}$$

where I is the peak-to-peak amplitude of the radical EPR signal, P is the microwave power, $P_{1/2}$ is the microwave power at half-saturation, b is the inhomogeneity parameter and A is a normalization constant [33]. The b value depends on the degree of inhomogeneous broadening of the EPR line which is determined by the ratio of the Lorentzian spin packet width and the Gaussian envelope width. Thus, b varies from 1.0 for the inhomogeneous to 2.0 for the homogeneous case. When log (I/P$^{1/2}$) is plotted versus log P, two linear regions are obtained that intersect at P = P$_{1/2}$ and the curve tends to a slope of b/2 under conditions of saturation.
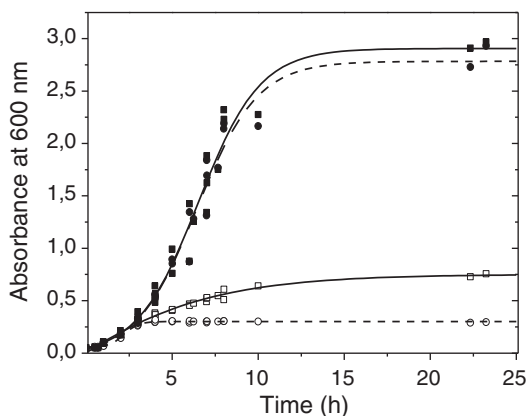
2.5. HYSCORE spectroscopy

2D HYSCORE experiments were carried out using a Bruker EleXsys E580 spectrometer equipped with an Oxford Instruments CF 935 cryostat. This four-pulse experiment (π/2-τ-π/2-t$_1$-π-t$_2$-π/2-τ-echo) was employed with appropriate phase-cycling schemes to eliminate

unwanted features from the experimental electron spin echo envelopes. The intensity of the echo after the fourth pulse was measured with varied t_2 and t_1 and constant τ. The length of a $\pi/2$ pulse was 16 ns and of a π pulse 32 ns. HYSCORE data were collected at 90 K in the form of 2D time-domain patterns containing 256×256 points with steps of 16 ns. Spectra were recorded at a magnetic field corresponding to the maximum intensity of the radical signal measured in a two-pulse field sweep electron spin echo sequence ($\pi/2$-τ-π-τ-echo). Spectra were processed using the Bruker Xepr software. Relaxation decays were subtracted (fitting by polynomial functions) followed by zero-filling and tapering with a Hamming window, before 2D Fourier transformation which finally gives the spectrum in frequency domain. Processed data were then imported into Matlab (The MathWorks Inc., Natick, MA) for plotting them. HYSCORE spectra are shown in absolute value mode and are presented as contour plots together with the skyline projection on the two frequency axes.

3. Results

3.1. DMK is a substrate of NarGHI in nitrate respiration

The participation of DMK to NarGHI-supported growth was evaluated using the *ubiE* strains. Indeed, *ubiE* encodes a C-methyltransferase which catalyzes not only the addition of a methyl group to the UQ precursor 2-octaprenyl-6-methoxy-1,4-benzoquinone (DDMQ-8) but also to the respiratory DMK (Fig. S1). Whereas, under aerobic growth conditions, the *ubiE* strain accumulates DDMQ-8 in addition to DMK as sole respiratory quinone [32,34], DDMQ-8 was almost undetectable under microaerophilic growth conditions (Fig. S2). While aerobic growth is strongly impaired in absence of *ubiE* owing to the absence of UQ, unaffected growth was observed under anoxic nitrate-respiring conditions as compared to the parental wild-type strain (Table S1). Identical results were obtained in a *ubiEA* strain which does not synthesize any DDMQ-8 (Table S1), establishing that the capacity of the *ubiE* strain to respire nitrate is provided by DMK-8. To evaluate the exact contribution of NarGHI to the DMK-supported growth under nitrate-respiring conditions, the experiment was repeated in the nitrate reductase-deficient JCB4023*ubiE* strain transformed with the pVA700 plasmid for which the use of NarGHI complex is mandatory for growth. Similar results were obtained with estimated generation time of 88 min for JCB4023/pVA700 and 84 min for JCB4023*ubiE*/pVA700 (Fig. 2). Thus, DMK is a substrate for NarGHI in nitrate respiration.

3.2. The NarGHI catalytic activity measured with the DMKH$_2$ analog 1,4-naphthoquinol is comparable to that measured using the corresponding methylated MKH$_2$ analog menadiol

To assess the influence of the methyl group at C2 position of the quinone ring on quinol:nitrate oxidoreductase activity, kinetic parameters for menadiol (MKH$_2$ analog) and 1,4-NQ (DMKH$_2$ analog) as substrates were determined on NarGHI-enriched IMVs from the JCB4023/pVA700 strain. The reaction follows Michaelis–Menten kinetics with respect to either quinol analogs. Table 2 summarizes the K_m, k_{cat} and k_{cat}/K_m data obtained from three independent determinations. Kinetic parameters for menadiol are similar to those previously published [30]. The K_m was identical for both quinol analogs demonstrating that the methyl group is not a key element for the binding of quinol analogs to NarGHI. However, the catalytic activity k_{cat} for menadiol is nearly 4-fold higher than that for 1,4-NQ. Thus, the k_{cat}/K_m parameters indicate that menadiol is a better substrate for NarGHI compared to 1,4-NQ.

To further understand the difference in reactivity, the redox potential of both quinol analogs are considered and reported in Table 2. $E'_{m,7.5}$ values of -30 and $+36$ mV can be indeed extrapolated for menadiol and 1,4-napththoquinol from measurements of their $E'_{m,7}$ in organic solvent and taking into account the pH difference and a variation of -60 mV/pH unit [14,35] (Table 2). A higher redox potential for 1,4-NQ is consistent with a reduced catalytic activity k_{cat} considering the $E_{m,7.5} \sim -10$ mV measured for the first electron acceptor, heme b_D (see Section 3.3).

3.3. DMSK intermediates are stabilized in NarGHI-enriched IMVs from a ubiE strain

The use of DMK by NarGHI raises the question of the ability of the enzyme to stabilize DMSK. To address this issue, NarGHI-enriched IMVs were purified from the DMK-only JCB4023*ubiE* strain, titrated and studied by EPR spectroscopy. An intense radical signal with an average g value $g_{av} \sim 2.0045$ is detected in the 0 to -100 mV range (Fig. 3). It is approximately 1.4 mT in overall peak-to-peak line width and exhibits a partially resolved splitting. This signal is not present in NarGHI-deficient IMVs prepared and titrated in similar conditions (Fig. 3D), demonstrating that the radical is specifically associated with the presence of NarGHI.

Careful examination of the radical EPR signal shape between 12 and 250 K reveals a relaxation behavior indicative of a non-composite signal (data not shown). Its saturation profile, obtained by measuring the peak-to-peak amplitude of the radical EPR signal at 150 K against microwave power, is shown in Fig. 4. It was measured at two different positions on the EPR line as indicated in the inset of Fig. 4. At each position, the saturation behavior is well fitted with a single saturation curve calculated from Eq. (4) using identical half-saturation microwave power $P_{1/2} = 0.18 \pm 0.02$ mW and slightly different inhomogeneity parameters $b = 1.51 \pm 0.02$ and 1.35 ± 0.02, for the narrow and large components, respectively (Fig. 4). This $P_{1/2}$ value is typical of slow relaxing semiquinone species [36] and is very close to the one previously reported by us on NarGHI-bound MSK using a similar analysis (i.e. $P_{1/2} = 0.22$ mW) [17]. In addition, this shows that the partially resolved splitting arises from a single radical species. This observation is corroborated by the unchanged shape of the radical EPR signal in the 0 to -200 mV range. This is illustrated on Fig. 3 where DMSK EPR

Fig. 2. DMK is a substrate for NarGHI in nitrate respiration. Growth curves of JCB4023 (squares) and JCB4023*ubiE* (circles) strains expressing NarGHI under nitrate-respiring conditions. Growth was performed under carbon-sufficient conditions (glycerol 137 mM, filled symbols) or under carbon-limitation (glycerol 1 mM, empty symbols). Growth curves represent the average of three independent cultures.

Table 2
Kinetic parameters of NarGHI with menadiol and 1,4-NQ as substrates. Redox potential values are taken from [14,35].

|	$E'_{m,7.5}$ (Q/QH$_2$) (mV)	K_m (μM)	k_{cat} (s^{-1})	k_{cat}/K_m (M^{-1}.s^{-1})
Menadiol	-31	71 ± 10	41 ± 2	5.8×10^5
1,4-NQ	34	65 ± 10	12 ± 1	1.8×10^5
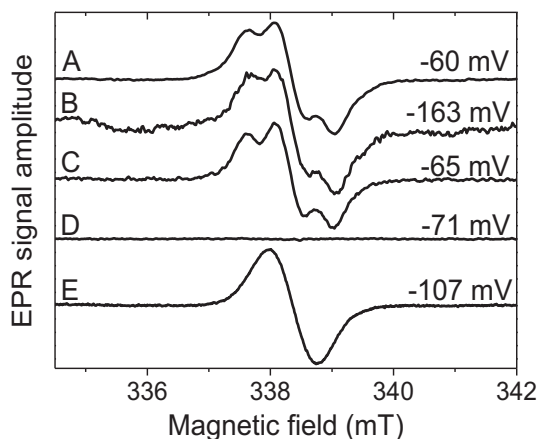
Fig. 3. Cw EPR spectra of purified IMVs from the following strains: A–C) IMVs from the NarGHI-enriched JCB4023*ubiE*/pVA700 strain containing DMK as sole respiratory quinone. In addition, IMVs in C) have been prepared in deuterium-exchanged buffer. D) IMVs from the nitrate reductase-deficient JCB4023*ubiE* strain. E) IMVs from the (UQ + MK + DMK) and NarGHI-enriched JCB4023/pVA700 strain. Other experimental conditions are: 60 K temperature, 0.1 mW microwave power, 9.4931 GHz microwave frequency, 0.3 mT magnetic field modulation amplitude at a frequency of 100 kHz. Samples were poised at a redox potential given in the figure. Spectra B, D and E have been normalized to the same maximum peak-to-peak amplitude as that of spectrum A.

spectra of samples redox-poised at -60 mV and -163 mV are shown (Fig. 3A & B, respectively). Finally, the radical titrates as a bell-shaped curve centered at ~-70 mV as expected for low-potential quinone species undergoing two successive one-electron transfer steps (Fig. 5).

Taken together, the EPR spectroscopic and redox properties of the radical detected in membrane fractions from the *ubiE* strain are fully consistent with the radical arising from a single NarGHI-bound semiquinone species. An identical radical EPR signal is also detected in a MG1655*ubiEA* strain, excluding it to arise from the previously mentioned UQ precursor, DDMQ-8 (Fig. S3). Therefore, the detected radical EPR signal is assigned to NarGHI-bound DMSK intermediates. When the titration data are fitted with theoretical curves based on Eq. (1), redox potential values $E_{1,7.5}$ (DMK/DMSK) $= -62 \pm 7$ mV and $E_{2,7.5}$ (DMSK/DMKH$_2$) $= -86 \pm 7$ mV are obtained giving $E'_{m,7.5}$ (DMK/DMKH$_2$) $= -74$ mV, a theoretical
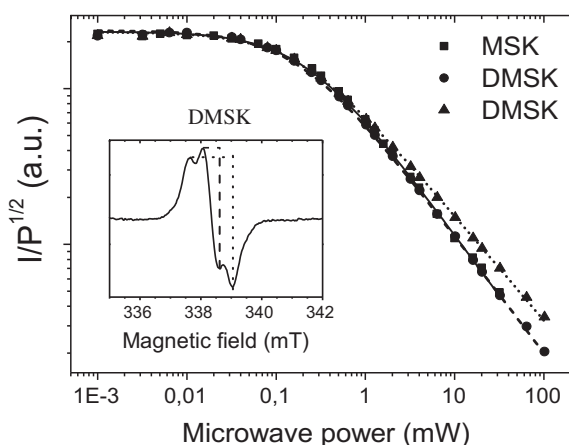
Fig. 4. Comparison of the microwave power saturation data of semiquinone signals recorded at 150 K in NarGHI-enriched IMVs from an *E. coli* JCB4023/pVA700 strain (squares, MSK) or a JCB4023*ubiE*/pVA700 strain (triangles and circles, DMSK) redox poised at -105 or -60 mV, respectively. For the later, the peak-to-peak amplitude I was measured at two positions on the EPR line as indicated in the spectrum shown in the inset (triangles, dotted lines; filled circles, dashed lines). To compare power saturation data, amplitudes of each data set were normalized to a value obtained by averaging the amplitudes of the three data sets measured in nonsaturating conditions (≤ 10 μW). Data points were fitted using Eq. (4) and $P_{1/2}$ and b values as given in the text.
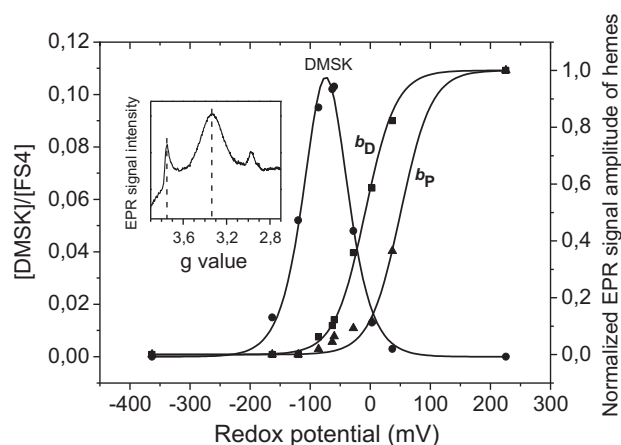
Fig. 5. EPR-monitored redox titrations of NarGHI-enriched IMVs obtained from the DMK-only JCB4023*ubiE* strain. The normalized ratio of the g = 2.0047 DMSK EPR signal intensity relative to that of FS4 (solid circles, left Y axis) and the normalized amplitudes of the g$_z$ component of the distal (g ~3.34, squares, right Y axis) and proximal (g ~3.75, triangles, right Y axis) hemes are plotted against the ambient redox potential. Solid lines are the best fits of experimental data points corresponding to one or two successive n = 1 redox processes and resulting from a least squares fitting procedure using either Eq. (1) or a n = 1 Nernst equation. Corresponding parameters are $E'^\circ_{7.5}$ (Fe^{3+}/Fe^{2+}) ~-10 and $\sim+50$ mV for hemes b_D and b_P, respectively or are reported in Table 3 for DMK. The inset shows the EPR spectrum of the two hemes poised at +226 mV. It was recorded at 12.5 K, 20 mW microwave power and 0.5 mT magnetic field modulation amplitude at a frequency of 100 kHz. Baseline drift is due to the presence of adventitious Fe^{3+} giving an isotropic signal at g = 4.3. The minor peak at g ~2.97 is associated to the presence of cytochrome bo_3 ubiquinol oxidase [37].

ratio [DMSK]$_{max}$/[Q$_D$ site] = 0.45 and a stability constant $K_{S,7.5}$ = 2.5 ($K_{S,7.5}$ in the range [1.5; 4.4]) calculated using Eq. (2) (Fig. 5 & Table 3). Spin quantitation shows that the maximum relative DMSK concentration is 0.11 ± 0.01 DMSK/Fe$_3$S$_4$ cluster (FS4) at pH 7.5, leading to an occupancy level $R_{occ,7.5}$ = 24 and $R_{occ,7.5}$ is in the range [19;32].

3.4. DMSK is formed at the NarGHI Q$_D$ quinol oxidation site

To gain insight into its binding mode to NarGHI, the DMSK radical species was studied using high resolution pulsed EPR methods at 90 K. At this temperature, the nuclear environment of the radical can be specifically probed without spectral contamination from other faster relaxing paramagnetic metal centers such as EPR-active cofactors in NarGHI [20]. The (+,+) quadrant of the low frequency part of a representative ^{14}N HYSCORE spectrum of DMSK is depicted in Fig. 6 (left). It exhibits the same correlation pattern as that observed for MSK (Fig. 6, right) and previously analyzed by us [20] i.e. two narrow off-diagonal peaks that correlate nuclear transition frequencies at 2.2 and 3.4 MHz. According to our previous work, these frequencies are assigned to the two double quantum transition frequencies ν_{dq+} = 3.4 MHz and ν_{dq-} = 2.2 MHz from a single ^{14}N nucleus weakly coupled to DMSK. No additional ^{14}N resonance is detected on other HYSCORE spectra of DMSK recorded at different τ values (not shown). Given that nuclear frequencies are very sensitive to the chemical nature of the nucleus, to its electrostatic environment and to the relative arrangement of the interacting electron/nuclear system, we conclude that DMSK and MSK interact with the same nitrogen-containing chemical group and in a similar manner. Thereof, characteristics of the detected DMSK/^{14}N interaction (calculated isotropic hyperfine coupling constant A$_{iso}$ ~0.8 MHz, quadrupole coupling constant κ and asymmetry parameter η that verify the relationships $\kappa^2 (3 + \eta^2) = 0.77$ MHz^2) are identical to those calculated in our previous study of the ^{14}N nucleus coupled to MSK or USQ, which was assigned to the N$_\delta$ imidazole nitrogen of the heme b_D axial ligand His66 (Fig. 1D) [16,20,22]. Altogether, these results demonstrate unambiguously that the NarGHI Q$_D$ site can stabilize and

Table 3

Comparison of the redox properties of NarGHI-bound or free MK, DMK and UQ at pH 7.5. "Free" refers to redox properties measured in alcoholic solvent or in bacterial membranes whereas "Q_D-bound state" refers to as measured when stabilized at the Q_D site of NarGHI. Literature data obtained at pH 7 have been extrapolated at pH 7.5 using a pH dependency of -60 mV/pH unit for E_m (Q/QH$_2$). The procedure used to estimate the redox parameters of Q_D-bound USQ is given in the Supplementary data.

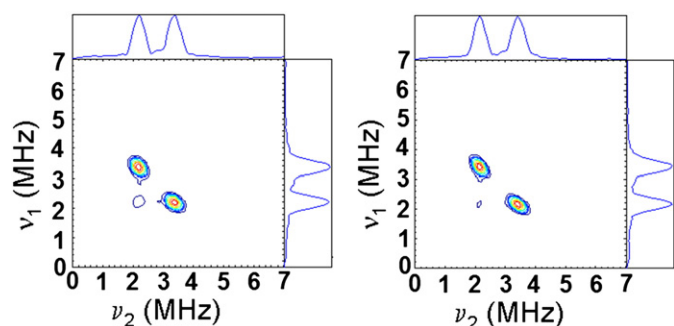|		E_1 (mV)	E_2 (mV)	E_m (mV)	K_S	R_{occ} (%)	Reference
DMSK	Free	–	–	$+6, -39$	–	–	[6,7]
	Q_D-bound	-62 ± 7	-86 ± 7	-74 ± 5	2.5[a]	24[b]	This work
MSK	Free	–	–	-100 ± 10	–	–	[35,38]
	Q_D-bound	-40 ± 10	-150 ± 10	-95 ± 5	73[c]	12[d]	[17]
USQ	Free	–	–	$+70 \pm 10$	–	–	[35,39]
	Q_D-bound	-40 to $+85$	$+35$ to $+160$	$+60 \pm 5$	4×10^{-4} to 7	n.d.	[16]

[a] $K_S \in [1.5–4.4]$.
[b] $R_{occ} \in [19–32]$.
[c] $K_S \in [33–158]$.
[d] $R_{occ} \in [10–15]$.

accommodate the semiquinone form of the three naturally-occurring respiratory quinones.

3.5. Origin of the partially resolved structure on the DMSK cw EPR signal

Simulation of the DMSK cw EPR signal assuming that the partially resolved structures arise from anisotropic g-tensor leads to g$_1$ = 2.0092 ± 0.0005, g$_2$ = 2.0049 ± 0.0005 and g$_3$ = 2.0003 ± 0.0005. Such g values are inconsistent with previously reported g-values of naphthosemiquinone species which lie in the range from 2.0021 to 2.0070 [17]. Thus, we assigned the partially resolved structure to interactions with another magnetic species, with a magnitude of ~15 MHz. We then envisage successively two possible origins, namely a spin–spin interaction with the unpaired electron of another nearby paramagnetic species, or a hyperfine coupling to a closely associated nuclear spin. Regarding the former possibility, a ~15 MHz coupling corresponds to a distance of ~15 Å between the interacting electron spins assuming a purely dipolar through-space interaction and a point dipole model. Whereas the NarH Fe$_4$S$_4$ clusters are expected to be too distant from the Q$_D$ site to give rise to such coupling, the contribution of the hemes was assessed by examining their redox behavior through EPR-monitored redox titrations. The two low-spin hemes exhibit highly anisotropic spectra with g$_z$ values of approximately 3.75 and 3.35 for heme b_P and b_D, respectively (Fig. 5, inset). Hemes b_D and b_P titrate as a single component that fits to n = 1 Nernstian curve with midpoint potential $E'_{m,7.5}$ ~−10 mV and +50 mV, respectively (Fig. 5), in consistency with previously published data [37,40]. Importantly, the EPR spectrum of NarGHI-bound DMSK is not affected by the redox state of the two hemes. In particular, the splitting on the DMSK EPR signal is clearly resolved in a sample redox poised at ~−163 mV (Fig. 3B) in

which the two NarGHI hemes are in their EPR-silent reduced state (Fig. 4). Moreover, a magnetic interaction between the radical and another paramagnetic species would lead not only to much higher P$_{1/2}$ value for DMSK than determined in the present work, but also would distort the saturation curves such that Eq. (4) would no longer model the data [41], a phenomenon that is clearly not observed here. We conclude that hemes b_D and b_P are not responsible for the partially resolved structure of the DMSK EPR signal. Thus, we assign the latter to a hyperfine structure which would originate from one or several nearby ^{1}H nuclei. Replacement of solvent water with ^{2}H$_2$O resulted only in a slight decrease of the EPR line width without changing its overall shape (Fig. 3C). The peak-to-peak line width of the central feature and the half width at half height of the left and right peaks of the DMSK EPR signal decrease by 0.1 mT, 0.04 mT and 0.05 mT, respectively, showing that the observed splitting originates from non-exchangeable protons coupled to DMSK. Moreover, the observed decrease of the line width also reveals the existence of at least one exchangeable proton weakly coupled to the radical, as previously shown for MSQ$_D$ [21].

4. Discussion

4.1. DMKH$_2$ is a substrate for nitrate respiration

Quinones are key players in energy-transducing processes which occur in the overwhelming majority of living organisms. The principal parameter distinguishing the different kinds of quinones is their midpoint redox potential. In this context, what makes the facultative anaerobe γ-proteobacterium E. coli an ideal system to probe the reactivity of quinones towards respiratory complexes is the coexistence of low- and high−redox potential quinones, MK-8 and UQ-8, respectively. Furthermore, E. coli marks out by the existence of a third quinone (DMK-8) of intermediate redox potential. In previous studies, the E. coli NarGHI complex was shown to stabilize semiquinone intermediates of both UQ-8 and MK-8 with the corresponding $E'_{m,7.5}$ of +60 and −90 mV, respectively [16–18]. The corresponding semiquinones were shown to be located at a single Q$_D$-site within the NarI subunit and to have a similar binding mode. Herein, we demonstrate that NarGHI can also make use of DMK as respiratory quinone for nitrate respiration and stabilizes a DMSK intermediate within its Q$_D$ site.

In agreement with the fact that DMK-8 predominates under nitrate-respiring conditions [12], this quinone allows efficient NarGHI-supported respiration with unchanged generation time as compared to wild-type strain. Whereas Wissenbach et al. reported that DMK-8 cannot support nitrate respiration in E. coli [11,13], our results show unambiguously that DMK-8 is a good substrate for NarGHI. Hence, the presence of the methyl group is not mandatory for efficient functioning of NarGHI-supported respiration. This is further confirmed by our observation that 1,4-NQ (a DMKH$_2$ analog) is only four-fold less efficient than menadiol (MKH$_2$ analog) as electron donor in enzymatic assays for nitrate reduction. Interestingly, Tyson et al. reported that DMKH$_2$ is not a substrate for the periplasmic nitrate reductase Nap complex in

Fig. 6. Comparison of ^{14}N HYSCORE spectra of DMSK (left) and MSK (right). Redox-poised samples (−60 mV for DMSK, −105 mV for MSK) issued from NarGHI-enriched membrane fractions from a JCB4023$ubiE$ (DMK) (left) or from a JCB4023 (DMK + MK + UQ) (right) E. coli strain were used. Experimental parameters are as given in Material and methods, time between first and second pulses τ = 204 ns, microwave frequency 9.69 GHz, and magnetic field 345.2 mT.

E. coli [42]. Quinone requirements for NarGHI and Nap would then be different, at least in *E. coli*. Indeed, nitrate respiration has been evidenced in the γ-proteobacterium *Haemophilus parainfluenzae* T3T1 [43] which contains (i) DMK as its sole respiratory quinone [44], (ii) no homologue to the *nar* operon, and (iii) an operon encoding a Nap enzyme. Overall, the ability of NarGHI to oxidize three types of quinols likely contributes to the large metabolic flexibility of *E. coli* upon sudden changes of the environmental conditions, in particular oxygen concentration.

4.2. A redox specific affinity of DMK to NarGHI

Using EPR-monitored redox titration experiments on NarGHI-enriched IMVs from a *ubiE* strain, we demonstrate unambiguously that DMSK is stabilized in NarGHI and resolve its redox properties. To our knowledge, stabilization of DMSK in an energy-transducing enzyme has not been reported so far. Whereas a $E'_{m,7}$ (MK/MKH$_2$) ~−70 ± 10 mV value of the n = 2 redox potential of menaquinones in organic solution or in a bacterial membrane at pH 7 is commonly used in the literature [35,38,45], that of the DMK/DMKH$_2$ couple has been recently challenged [7]. Loss of the methyl group at the C2 position of the menaquinone ring is expected to significantly increase the E_m (Q/QH$_2$) value with respect to that of the methylated species [46,47]. Consistently, the midpoint potential of 1,4-NQ is ~65 mV higher than that of menadione (Table 2) [14,35]. Regarding DMK, two different $E'_{m,7}$ (DMK/DMKH$_2$) values have been reported from measurements carried out in alcoholic solvent, namely + 36 mV [6] and − 9 mV [7]. Assuming that the DMK pool in membranes has a similar E'_m value and that the latter changes by − 60 mV/pH unit as previously measured [7], our data reveal that the $E'_{m, 7.5}$ (DMK/DMKH$_2$) = − 74 mV value for NarGHI-bound species (Table 3) results from a negative shift Δ = − 30 or − 80 mV, depending on the $E'_{m,7}$ value considered for unbound DMK. A positive shift of the same order of magnitude has been observed for USQ stabilized at the quinone reduction site of either succinate–ubiquinone reductase (Δ ~+ 20 mV) [48] or of the bc_1 complex from yeast (Δ ~+ 24 to + 54 mV) [49] or from *Rhodobacter sphaeroides* (Δ ~+ 60 mV) [50]. A redox-dependent differential binding of quinone at these sites has been proposed as a possible explanation of this shift. Whereas a positive shift predicts a stronger affinity of the hydroquinone form with respect to the quinone form, the negative one observed for NarGHI-bound DMSK indicates tighter binding of oxidized DMK than DMKH$_2$ to the Q$_D$ site (15-fold or ~500-fold depending on the $E'_{m,7}$ value considered for unbound DMK) Eq. (3). Remarkably, this phenomenon is specific to DMSK as no shift is observed neither for NarGHI-bound MSK [17, 38], nor for NarGHI-bound USQ [16] (Table 3). Since our ^{14}N HYSCORE investigations show that the three quinone species bind to the NarGHI Q$_D$ site via a similar His-SQ binding motif, it is likely that the H-bonding pattern to these radicals is similar, at least to the O1 carbonyl oxygen. This situation recalls that observed for quinones stabilized in the Q site of cytochrome *bd*-I (CydAB) or in the modified Q site of the FrdC E29L fumarate reductase mutant. These two respiratory complexes have been shown to react with both menaquinols and ubiquinols. Whereas their Q sites do not discriminate between benzoquinones and benzoquinols (CydAB) [51], or ubiquinones and ubiquinols (FrdC E29L) [52], a positive shift ~35–40 mV of E_m is however resolved for protein-bound naphthoquinols (CydAB) or menaquinols (FrdC E29L) with respect to unbound species. In both protein Q sites, MK and UQ appear to have a similar hydrogen bonding to one of their quinone carbonyl group (as observed here for the three types of NarGHI-bound semiquinones) as evaluated by FTIR difference spectroscopy [52,53]. However, it has been hypothesized that differences in the protonation of the two quinone species involve the other quinone carbonyl group and/or a nearby acidic residue. Whether this applies to NarGHI-bound DMSK, MSK and USQ requires further investigations. High resolution EPR experiments are currently performed in our labs

to attempt to resolve this issue. In particular, the possible differential role of Lys 86 located at the entrance of the Q$_D$ site is being assessed.

To evaluate the physiological impact of the redox-dependent differential binding of DMK *in vivo*, we anticipate that reducing the availability of the carbon source with unchanged nitrate concentration would unbalance the electron flux resulting in a more oxidized DMK Q pool. Under such conditions, deletion of the *ubiE* gene is expected to influence the growth as compared to the wild-type strain. As seen in Fig. 2, lowering down the glycerol concentration to 1 mM not only reduces the overall growth yield due to carbon limitation but significantly hampers the growth of the *ubiE* strain as expected. Thereof, under such nutrient-limited conditions, DMK utilization is not favored for NarGHI-dependent nitrate respiration. To conclude, these *in vivo* results substantiate the redox-dependent differential binding of DMK inferred from EPR-monitored redox titration experiments.

4.3. Evaluation of the functional consequences of the differential redox properties of MK-8, DMK-8 and UQ-8 at the NarGHI Q$_D$ site

Our previous characterization of NarGHI-bound MSK was carried out using a wild-type bacterial strain containing the three physiological respiratory quinones [17]. In light of the present work, re-examination of the previously recorded EPR spectra of MSK reveals that DMSK does not contribute in this sample (see SI material). Thus, the MSK EPR redox properties recalled in Table 3 can be reliably compared to those of DMSK. Notably, the present work reveals that the NarGHI complex is unique in being able to stabilize the semiquinone intermediate of all three respiratory quinones from *E. coli* within a single Q$_D$-site. Thanks to the availability of distinct redox properties for DMSK and MSK, we questioned whether NarGHI exhibits distinct specificity towards the considered quinones. A definitive answer cannot be provided *in vivo* through assessment of the generation time since the resulting activity of several electron transfer chains ending up with NarGHI are at play under our growth conditions. Furthermore, MK-8-exclusive growth cannot be performed, as DMK is the precursor of MK. Instead, we have evaluated the theoretical kinetics of electron transfer at the Q$_D$ site based on the herein reported redox properties of bound DMSK and MSK. A relative short distance of 5.7 Å can be estimated between the carbonyl of the semiquinone involved in hydrogen-bonding with the His66 residue and the porphyrin ring of heme b_D. As a consequence, based on the Moser–Dutton model (see SI text, Eq. S1) [55], very fast kinetics (between 4 and 15 ns^{-1}) are expected to occur during the two successive oxidation steps of MKH$_2$ and DMKH$_2$ at the Q$_D$ site. The situation may even be more complicated for the utilization of UQ-8 by NarGHI with an $E'_{m,7.5}$ (UQ/UQH$_2$) at the Q$_D$ site measured at ~60 mV (Table 3) [16]. Whereas the overlapping USQ signal originating from other respiratory complexes precludes accurate determination of the two n = 1 redox potential values, limit values can be given considering either that USQ$_D$ predominates or is very minor in the previously studied sample (see SI text and ref. [16]) ending up with K_S values of 7 or 4×10^{-4}, respectively. In the first case, much slower kinetics (between 50 and 130 μs^{-1}) are calculated for the two successive oxidation steps of UQH$_2$ at the Q$_D$ site. These values are nearly two-fold lower than those measured for MKH$_2$ and DMKH$_2$. In the other opposite case, the very low stability constant resulting from the inversion of the two n = 1 redox potentials severely impacts the first oxidation step QH$_2$/SQ with an estimated value of 9 μs^{-1} while the second step is facilitated at 4 ns^{-1}. It is worth to mention that transmembrane electron transfer between both hemes within NarI is severely hampered by the small redox potential difference (Δ ~60 mV) between them further reduced by the membrane potential Δψ ~130 mV [56]. With a distance of 8.7 Å between both hemes, unoriented electron transfer kinetics is estimated between 18 and 36 μs^{-1} depending on the midpoint potential values of both hemes in the literature. Further experiments are required to evaluate whether this may constitute a limiting step for UQ utilization. Overall, under highly reducing conditions, undistinguished kinetics is

expected to occur with MK or DMK as substrate. In the case of UQ, one can anticipate a less efficient use of this substrate which may corroborate the longer generation time obtained in a UQ-only strain under nitrate respiring conditions (Table S1).

4.4. Different stabilization of MSK and DMSK in the NarGHI Q_D site

The measured differences between the MSK and DMSK redox properties (Table 3) imply an approximately two-fold lower maximal DMSK concentration compared to that of MSK (as calculated using Eq. (1) assuming the same occupation level). Spin quantitation experiments reveal that the maximal SQ spin concentration relative to that of FS4 is similar for both species (i.e. 0.11 ± 0.01 DMSK/FS4 and 0.10 ± 0.01 MSK/FS4) [54]. Therefore, a two-fold higher Q_D site occupancy level of DMK (19 to 32%) as compared to MK (10 to 15%) is calculated using Eq. (1) (Table 3) [54]. This variation could be due to difference in the availability of the two quinone types in the two preparations or to a differential affinity of DMK for this site compared to MK consecutive to the loss of the methyl group on the ring moiety. Finally, to understand the molecular origin of the differences observed in the stability constant for both MSK and DMSK, further detailed studies aimed at deciphering the DMSK binding mode to the protein are currently underway in our labs using multifrequency high resolution EPR techniques. In particular, the origin of the hyperfine splitting observed on the DMSK EPR spectrum is currently being investigated.

5. Conclusions

In this work, we report the efficient use of DMK by *E. coli* in nitrate respiration *in vivo*. Further, we demonstrate that DMSK intermediates are stabilized in the NarGHI quinol oxidation site Q_D, allowing the first redox characterization of a protein-bound DMSK.

Transparency document

The Transparency document associated with this article can be found, in the online version.

Appendix A. Supplementary data

Supplementary data to this article can be found online at http://dx.doi.org/10.1016/j.bbabio.2015.05.001.

References

[1] B. Schoepp-Cothenet, R. van Lis, A. Atteia, F. Baymann, L. Capowiez, A.L. Ducluzeau, S. Duval, F. Ten Brink, M.J. Russell, W. Nitschke, On the universal core of bioenergetics, Biochim. Biophys. Acta 1827 (2012) 79–93.

[2] D.J. Richardson, Bacterial respiration: a flexible process for a changing environment, Microbiology 146 (Pt 3) (2000) 551–571.

[3] G. Unden, P. Steinmetz, P. Degreif-Dünnwald, The Aerobic and Anaerobic Respiratory Chain of *Escherichia* coli and *Salmonella* enterica: Enzymes and Energetics, EcoSal Plus (2014), http://dx.doi.org/10.1128/ecosalplus.

[4] G. Unden, J. Bongaerts, Alternative respiratory pathways of *Escherichia coli*: energetics and transcriptional regulation in response to electron acceptors, Biochim. Biophys. Acta 1320 (1997) 217–234.

[5] B. Nowicka, J. Kruk, Occurrence, biosynthesis and function of isoprenoid quinones, Biochim. Biophys. Acta 1797 (2010) 1587–1605.

[6] R. Hollander, Correlation of the function of demethylmenaquinone in bacterial electron transport with its redox potential, FEBS Lett. 72 (1976) 98–100.

[7] P. Infossi, E. Lojou, J.-P. Chauvin, G. Herbette, M. Brugna, M.-T. Giudici-Orticoni, *Aquifex aeolicus* membrane hydrogenase for hydrogen biooxidation: role of lipids and physiological partners in enzyme stability and activity, Int. J. Hydrog. Energy 35 (2010) 10778–10789.

[8] P. Sharma, M.J. Teixeira de Mattos, K.J. Hellingwerf, M. Bekker, On the function of the various quinone species in *Escherichia coli*, FEBS J. 279 (2012) 3364–3373.

[9] A.I. Shestopalov, A.V. Bogachev, R.A. Murtazina, M.B. Viryasov, V.P. Skulachev, Aeration-dependent changes in composition of the quinone pool in *Escherichia coli*. Evidence of post-transcriptional regulation of the quinone biosynthesis, FEBS Lett. 404 (1997) 272–274.

[10] M. Bekker, G. Kramer, A.F. Hartog, M.J. Wagner, C.G. de Koster, K.J. Hellingwerf, M.J. de Mattos, Changes in the redox state and composition of the quinone pool of *Escherichia coli* during aerobic batch-culture growth, Microbiology 153 (2007) 1974–1980.

[11] B.J. Wallace, I.G. Young, Role of quinones in electron transport to oxygen and nitrate in *Escherichia coli*. Studies with a ubiA-menA-double quinone mutant, Biochim. Biophys. Acta 461 (1977) 84–100.

[12] G. Unden, Differential roles for menaquinone and demethylmenaquinone in anaerobic electron transport of *E. coli* and their fnr-independent expression, Arch. Microbiol. 150 (1988) 499–503.

[13] U. Wissenbach, D. Ternes, G. Unden, An *Escherichia coli* mutant containing only demethylmenaquinone, but no menaquinone: effects on fumarate, dimethylsulfoxide, trimethylamine N-oxide and nitrate respiration, Arch. Microbiol. 158 (1992) 68–73.

[14] U. Wissenbach, A. Kroger, G. Unden, The specific functions of menaquinone and demethylmenaquinone in anaerobic respiration with fumarate, dimethylsulfoxide, trimethylamine N-oxide and nitrate by *Escherichia coli*, Arch. Microbiol. 154 (1990) 60–66.

[15] M.G. Bertero, R.A. Rothery, M. Palak, C. Hou, D. Lim, F. Blasco, J.H. Weiner, N.C. Strynadka, Insights into the respiratory electron transfer pathway from the structure of nitrate reductase A, Nat. Struct. Biol. 10 (2003) 681–687.

[16] R. Arias-Cartin, S. Lyubenova, P. Ceccaldi, T. Prisner, A. Magalon, B. Guigliarelli, S. Grimaldi, HYSCORE evidence that endogenous mena- and ubisemiquinone bind at the same Q site (Q_D) of *Escherichia coli* nitrate reductase A, J. Am. Chem. Soc. 132 (2010) 5942–5943.

[17] S. Grimaldi, P. Lanciano, P. Bertrand, F. Blasco, B. Guigliarelli, Evidence for an EPR-detectable semiquinone intermediate stabilized in the membrane-bound subunit NarI of nitrate reductase A (NarGHI) from *Escherichia coli*, Biochemistry 44 (2005) 1300–1308.

[18] P. Lanciano, A. Magalon, P. Bertrand, B. Guigliarelli, S. Grimaldi, High-stability semiquinone intermediate in nitrate reductase A (NarGHI) from *Escherichia coli* is located in a quinol oxidation site close to heme b_D, Biochemistry 46 (2007) 5323–5329.

[19] S. Grimaldi, B. Schoepp-Cothenet, P. Ceccaldi, B. Guigliarelli, A. Magalon, The prokaryotic Mo/W-*bis*PGD enzymes family: a catalytic workhorse in bioenergetic, Biochim. Biophys. Acta 1827 (2013) 1048–1085.

[20] S. Grimaldi, R. Arias Cartin, P. Lanciano, S. Lyubenova, B. Endeward, T.F. Prisner, A. Magalon, B. Guigliarelli, Direct evidence for nitrogen ligation to the high-stability semiquinone intermediate in *Escherichia coli* nitrate reductase A, J. Biol. Chem. 285 (2010) 179–187.

[21] S. Grimaldi, R. Arias-Cartin, P. Lanciano, S. Lyubenova, R. Szenes, B. Endeward, T.F. Prisner, B. Guigliarelli, A. Magalon, Determination of the proton environment of high stability menasemiquinone intermediate in *Escherichia coli* nitrate reductase A by pulsed EPR, J. Biol. Chem. 287 (2012) 4662–4670.

[22] M.G. Bertero, R.A. Rothery, N. Boroumand, M. Palak, F. Blasco, N. Ginet, J.H. Weiner, N.C. Strynadka, Structural and biochemical characterization of a quinol binding site of *Escherichia coli* nitrate reductase A, J. Biol. Chem. 280 (2005) 14836–14843.

[23] T. Baba, T. Ara, M. Hasegawa, Y. Takai, Y. Okumura, M. Baba, K.A. Datsenko, M. Tomita, B.L. Wanner, H. Mori, Construction of *Escherichia coli* K-12 in-frame, single-gene knockout mutants: the Keio collection, Mol. Syst. Biol. 2 (2006) (2006) 0008.

[24] L.C. Potter, P. Millington, L. Griffiths, G.H. Thomas, J.A. Cole, Competition between *Escherichia coli* strains expressing either a periplasmic or a membrane-bound nitrate reductase: does Nap confer a selective advantage during nitrate-limited growth? Biochem. J. 344 (Pt 1) (1999) 77–84.

[25] K.A. Datsenko, B.L. Wanner, One-step inactivation of chromosomal genes in *Escherichia coli* K-12 using PCR products, Proc. Natl. Acad. Sci. U. S. A. 97 (2000) 6640–6645.

[26] B. Guigliarelli, A. Magalon, M. Asso, P. Bertrand, C. Frixon, G. Giordano, F. Blasco, Complete coordination of the four Fe–S centers of the beta subunit from *Escherichia coli* nitrate reductase. Physiological, biochemical, and EPR characterization of site-directed mutants lacking the highest or lowest potential [4Fe–4S] clusters, Biochemistry 35 (1996) 4828–4836.

[27] O.H. Lowry, N.J. Rosebrough, A.L. Farr, R.J. Randall, Protein measurement with the Folin phenol reagent, J. Biol. Chem. 193 (1951) 265–275.

[28] V. Augier, B. Guigliarelli, M. Asso, P. Bertrand, C. Frixon, G. Giordano, M. Chippaux, F. Blasco, Site-directed mutagenesis of conserved cysteine residues within the beta subunit of *Escherichia coli* nitrate reductase. Physiological, biochemical, and EPR characterization of the mutated enzymes, Biochemistry 32 (1993) 2013–2023.

[29] V. Augier, M. Asso, B. Guigliarelli, C. More, P. Bertrand, C.L. Santini, F. Blasco, M. Chippaux, G. Giordano, Removal of the high-potential [4Fe–4S] center of the beta-subunit from *Escherichia coli* nitrate reductase. Physiological, biochemical, and EPR characterization of site-directed mutated enzymes, Biochemistry 32 (1993) 5099–5108.

[30] J. Buc, C.L. Santini, F. Blasco, R. Giordani, M.L. Cardenas, M. Chippaux, A. Cornish-Bowden, G. Giordano, Kinetic studies of a soluble alpha beta complex of nitrate reductase A from *Escherichia coli*. Use of various alpha beta mutants with altered beta subunits, Eur. J. Biochem. 234 (1995) 766–772.

[31] R.W. Jones, P.B. Garland, Sites and specificity of the reaction of bipyridylium compounds with anaerobic respiratory enzymes of *Escherichia coli*. Effects of permeability barriers imposed by the cytoplasmic membrane, Biochem. J. 164 (1977) 199–211.

[32] M. Hajj Chehade, L. Loiseau, M. Lombard, L. Pecqueur, A. Ismail, M. Smadja, B. Golinelli-Pimpaneau, C. Mellot-Draznieks, O. Hamelin, L. Aussel, S. Kieffer-Jaquinod, N. Labessan, F. Barras, M. Fontecave, F. Pierrel, ubiI, a new gene in *Escherichia coli* coenzyme Q biosynthesis, is involved in aerobic C5-hydroxylation, J. Biol. Chem. 288 (2013) 20085–20092.

[33] H. Rupp, K.K. Rao, D.O. Hall, R. Cammack, Electron spin relaxation of iron–sulphur proteins studied by microwave power saturation, Biochim. Biophys. Acta 537 (1978) 255–260.

[34] P.T. Lee, A.Y. Hsu, H.T. Ha, C.F. Clarke, A C-methyltransferase involved in both ubiquinone and menaquinone biosynthesis: isolation and identification of the *Escherichia coli* ubiE gene, J. Bacteriol. 179 (1997) 1748–1754.

[35] U. Schnorf, Der Einfluss von Substitutenten auf Redoxpotentiale und Wuchsstoffeigenschaften von Chinonen(doctoral thesis) ETH Zürich, 1966.

[36] W.J. Ingledew, T. Ohnishi, J.C. Salerno, Studies on a stabilisation of ubisemiquinone by *Escherichia coli* quinol oxidase, cytochrome *bo*, Eur. J. Biochem. 227 (1995) 903–908.

[37] J.G. Fedor, R.A. Rothery, K.S. Giraldi, J.H. Weiner, Q-site occupancy defines heme heterogeneity in *Escherichia coli* nitrate reductase A (NarGHI), Biochemistry 53 (2014) 1733–1741.

[38] U. Liebl, S. Pezennec, A. Riedel, E. Kellner, W. Nitschke, The Rieske FeS center from the gram-positive bacterium PS3 and its interaction with the menaquinone pool studied by EPR, J. Biol. Chem. 267 (1992) 14068–14072.

[39] K.I. Takamiya, P.L. Dutton, Ubiquinone in *Rhodopseudomonas sphaeroides*. Some thermodynamic properties, Biochim. Biophys. Acta 546 (1979) 1–16.

[40] R.A. Rothery, F. Blasco, J.H. Weiner, Electron transfer from heme b_L to the [3Fe–4S] cluster of *Escherichia coli* nitrate reductase A (NarGHI), Biochemistry 40 (2001) 5260–5268.

[41] C. Galli, J.B. Innes, D.J. Hirsh, G.W. Brudvig, Effects of dipole–dipole interactions on microwave progressive power saturation of radicals in proteins, J. Magn. Reson. B 110 (1996) 284–287.

[42] K. Tyson, R. Metheringham, L. Griffiths, J. Cole, Characterisation of *Escherichia coli* K-12 mutants defective in formate-dependent nitrite reduction: essential roles for hemN and the menFDBCE operon, Arch. Microbiol. 168 (1997) 403–411.

[43] P.R. Sinclair, D.C. White, Effect of nitrate, fumarate, and oxygen on the formation of the membrane-bound electron transport system of *Haemophilus parainfluenzae*, J. Bacteriol. 101 (1970) 365–372.

[44] R.K. Hammond, D.C. White, Separation of vitamin K2 isoprenologues by reversed-phase thin-layer chromatography, J. Chromatogr. 45 (1969) 446–452.

[45] R.K. Thauer, K. Jungermann, K. Decker, Energy conservation in chemotrophic anaerobic bacteria, Bacteriol. Rev. 41 (1977) 100–180.

[46] W.M. Clark, Oxidation–Reduction Potentials of Organic Systems, Williams & Wilkins, Baltimore, 1960.

[47] A. Brunmark, E. Cadenas, Redox and addition chemistry of quinoid compounds and its biological implications, Free Radic. Biol. Med. 7 (1989) 435–477.

[48] T. Miki, L. Yu, C.A. Yu, Characterization of ubisemiquinone radicals in succinate–ubiquinone reductase, Arch. Biochem. Biophys. 293 (1992) 61–66.

[49] R. Covian, K. Zwicker, F.A. Rotsaert, B.L. Trumpower, Asymmetric and redox-specific binding of quinone and quinol at center N of the dimeric yeast cytochrome bc1 complex. Consequences for semiquinone stabilization, J. Biol. Chem. 282 (2007) 24198–24208.

[50] D.E. Robertson, R.C. Prince, J.R. Bowyer, K. Matsuura, P.L. Dutton, T. Ohnishi, Thermodynamic properties of the semiquinone and its binding site in the ubiquinol–cytochrome c (c_2) oxidoreductase of respiratory and photosynthetic systems, J. Biol. Chem. 259 (1984) 1758–1763.

[51] S.F. Hastings, T.M. Kaysser, F. Jiang, J.C. Salerno, R.B. Gennis, W.J. Ingledew, Identification of a stable semiquinone intermediate in the purified and membrane bound ubiquinol oxidase–cytochrome *bd* from *Escherichia coli*, Eur. J. Biochem. 255 (1998) 317–323.

[52] E. Maklashina, P. Hellwig, R.A. Rothery, V. Kotlyar, Y. Sher, J.H. Weiner, G. Cecchini, Differences in protonation of ubiquinone and menaquinone in fumarate reductase from *Escherichia coli*, J. Biol. Chem. 281 (2006) 26655–26664.

[53] J. Zhang, W. Oettmeier, R.B. Gennis, P. Hellwig, FTIR spectroscopic evidence for the involvement of an acidic residue in quinone binding in cytochrome *bd* from *Escherichia coli*, Biochemistry 41 (2002) 4612–4617.

[54] R. Arias-Cartin, S. Grimaldi, J. Pommier, P. Lanciano, C. Schaefer, P. Arnoux, G. Giordano, B. Guigliarelli, A. Magalon, Cardiolipin-based respiratory complex activation in bacteria, Proc. Natl. Acad. Sci. U. S. A. 108 (2011) 7781–7786.

[55] C.C. Page, C.C. Moser, X. Chen, P.L. Dutton, Natural engineering principles of electron tunnelling in biological oxidation–reduction, Nature 402 (1999) 47–52.

[56] Q.H. Tran, G. Unden, Changes in the proton potential and the cellular energetics of *Escherichia coli* during growth by aerobic and anaerobic respiration or by fermentation, Eur. J. Biochem. 251 (1998) 538–543.